Electronic Supplementary Material (ESI) for Chemical Communications.

Supporting Information

Dendritic Core-shell Cu@PtCu Alloy Electrocatalyst Resulting in Enhanced Electron Transfer Ability and Boosted Surface Active Sites for Improved Methanol Oxidation Reaction

Jiayin Liu, [+a,b] Guangran Xu,[+a,b] Baocang Liu[a,b] and Jun Zhang*[a,b]

[a]College of Chemistry and Chemical Engineering, Inner Mongolia University, Hohhot 010021, P. R. China

[b]Inner Mongolia Key Lab of Nanoscience and Nanotechnology, Inner Mongolia University, Hohhot 010021, P. R. China

[+]Equal contribution to the paper

*Corresponding author: Prof. J. Zhang, Email: cejzhang@imu.edu.cn

1. Experimental section

1.1. Chemicals and Materials

Platinum acetylacetonate ($Pt(acac)_2$, 98%), copper acetylacetonate ($Cu(acac)_2$), N,N-dimethylformamide (DMF), poly (vinylpyrrolidone) (PVP, MW = 58 000), glycine (Gly) and NaBr were purchased from Acros. Hydrazine hydrate (HHA), ascorbic acid (AA), and sodium borohydride (SBH) were purchased from Alfa Aesar. Sulfuric acid (H_2SO_4, 70 %) and Nafion (5 wt%) were purchased from Sigma–Aldrich. All aqueous solutions were prepared using deionized water.

1.2. Synthesis of Cu@PtCuGly alloy electrocatalyst

To synthesize Cu@PtCu alloy electrocatalyst, 210 mg of PVP, 91 mg of $Pt(acac)_2$, and 40.6 mg

of $Cu(acac)_2$ with a theoretical molar ratio of Pt:Cu at 3:2 were first dissolved in 12 mL of DMF. After stirring 5 min, 1 g of NaBr and 25.55 mg of glycine (Gly) pre-dissolved in 1 mL of H_2O were added in the above solution, which was further stirred for 15 min. The obtained mixture solution was further sonicated in an ultrasonic bath for 5 min at room temperature to form homogeneous blue solution. Subsequently, the solution was transferred to a 25 mL Teflon-lined stainless-steel autoclave and heated at 180 °C for 4 h before it was cooled to room temperature naturally. Finally, the Cu@PtCu alloy nanocrystals were collected by centrifugation (12000 rpm for 15 min), and then washed several times with a mixture of ethanol and water at a volume ration of 1:1 to remove impurities and then stored for further characterization. The obtained Cu@PtCu alloy electrocatalyst obtained using Gly as reductant was nominated as Cu@PtCu(Gly).

To understand the effect of surface N doping arisen from the reduction of N-contained reductants on the catalytic performance, the Cu@PtCu(Gly) nanocrystals was added into a mixture of ethanol and water at a volume ration of 1:1 in a 100 mL beaker and the solution was vigorously stirred for 24 h. Then, the catalysts were centrifuged at 12000 rpm for 10 min and dried in a vacuum oven for 6 h at 50 °C. The obtained sample was nominated as post-treated Cu@PtCu(Gly).

1.3. Synthesis of PtCu(HHA), PtCu(AA) and PtCu(SBH) alloy electrocatalysts

The synthesis of PtCu (HHA), PtCu (AA) and PtCu (SBH) alloy electrocatalysts followed the similar synthetic procedures except using the similar ratio of hydrazine hydrate (HHA), ascorbic acid (AA), and sodium borohydride (SBH) to replace Gly as reductants and, correspondingly, the obtained PtCu alloy electrocatalysts obtained using HHA, AA, and SBH

as reductants were nominated as PtCu(HHA), PtCu(AA), and PtCu(SBH), respectively.

1.4. Characterization

Scanning transmission electron microscopy (STEM) and transmission electron microscopy (TEM) characterizations were performed on a FEI Tecnai F20 field-emission transmission electron microscope (FE-TEM) system with an energy dispersive spectrometer (EDS) for elemental analyses. X-ray powder diffraction (XRD) was performed on a PANalytical Empyrean diffractometer with Cu Kalpha1 radiation (λ = 1.5405 Å) in the Bragg angle ranging between 20° and 80°. X-ray photoelectron spectroscopy (XPS) measurements were performed in a VG Scientific ESCALAB Mark II spectrometer equipped with two ultrahigh vacuum (UHV) chambers. The inductively coupled plasma optical emission spectrometry (ICP-OES) analysis was conducted using a Thermo Scientific iCAP6300 (Thermo Fisher Scientific, US).

1.5. Electrochemical tests

Electrochemical measurements were carried out with a three electrode system on a CHI 600C electrochemical analyzer (CH Instrument, China). A platinum wire, an Ag/AgCl, and a glassy carbon electrode (GCE, 3 mm in diameter) modified by catalyst were used as the counter, reference and working electrode, respectively. The working electrode was coated with different catalysts with the same loading amount of 2 μg and dried at room temperature. MOR measurements were performed in a 0.5 M N_2-saturated H_2SO_4 solution containing 1 M methanol at a scan rate of 50 $mV \cdot s^{-1}$. The electrochemical active surface area (ECSA) measurements were determined by integrating the hydrogen adsorption charge on the cyclic voltammetry (CV) at room temperature in nitrogen saturated 0.5 M H_2SO_4 solution

with a scan rate of 50 mV/s. The ECSAs were calculated by the following equation: ECSA = QH/m × 210, where QH is the charge for Hupd adsorption determined using QH = 0.5 × Q (where Q is the charge in the Hupd adsorption–desorption area obtained after the double layer correction region between 0 and 0.37 V), m is the Pt loading amount on the electrode, and 210 $\mu C \cdot cm^{-2}$ is the charge required for the monolayer adsorption of hydrogen on the Pt surface.

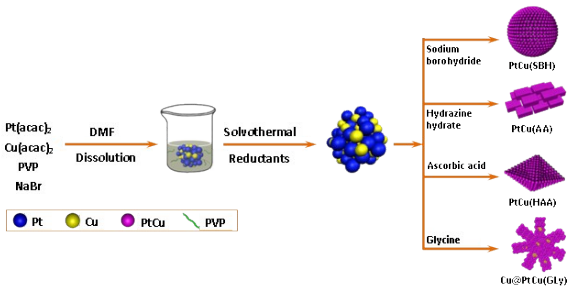

Scheme S1. Schematic illustration showing the formation of dendritic core-shell Cu@PtCu and PtCu alloy nanocrystals using different reducing agents.

The formation of dendritic core-shell Cu@PtCu(Gly) involves several steps and each step is well controlled (Scheme S1). In the initial formation stage, Cu and Pt precursors are reduced to form Pt and Cu seeds, which gradually grow into a cladding structure under hydrothermal condition. Next, following the continuous heating treatment, rod-like PtCu alloy nanocrystals are formed and simultaneously assembled on Cu seeds. Ultimately, these PtCu alloy nanocrystals are transformed into dendritic morphologies *via* self-assembly on Cu cores to form dendritic core-shell Cu@PtCu(Gly) alloy nanocrystals. Due to the stronger reduction of HHA, AA, and SBH than Gly, the Pt and Cu precursors are reduced simultaneously to form PtCu alloys without Cu cores.

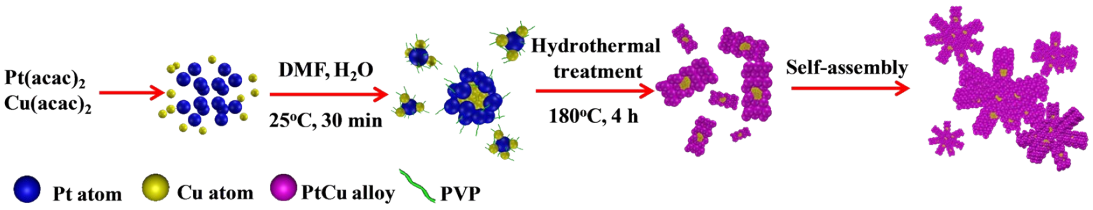

Scheme S2. Schematic illustration shows the formation process of dendritic core-shell Cu@PtCu(Gly) alloy electrocatalyst.

Table S1. XPS binding energies for Pt $4f_{7/2}$, Cu $2p_{3/2}$, N1s for pyrrolic N and pyridinic N of different electrocatalysts.

Electrocatalyst	Binding energies			
	$Pt4f_{2/7}$	$Cu2p_{3/2}$	Pyrrolic N	Pyridinic N
Cu@PtCu(Gly)	71.029	931.800	399.59	397.30
PtCu(HHA)	71.070	931.900	399.69	397.80
PtCu(AA)	71.020	931.900	400.00	397.65
PtCu(SBH)	71.270	932.100	399.90	397.80
Post-treated Cu@PtCu(Gly)	71.190	931.770	400.10	397.30

Table S2. The actual contents of Pt, Cu, and N in different electrocatalysts calculated according to the ICP and XPS measurements.

Electrocatalyst (theoretical Pt/Cu = 3:2)	Total Pt	Total Cu	Total N	Pt^0	Pt^{2+}	Pt^{4+}	Cu^0	Cu^{2+}	Pyrrolic N	Pyridinic N
	Measured by ICP / %			Calculated by XPS / %						
Cu@PtCu(Gly)	18.8	16.5	25.4	80.9	9.8	9.3	82.7	17.3	93.1	6.9
PtCu(HHA)	21.9	20.7	22.2	75.5	13.9	10.6	71.5	28.5	92.5	7.5
PtCu(AA)	26.5	19.2	20.2	74.8	13．0	12.2	88.5	11.5	77.1	22.9
PtCu(SBH)	28.3	23.2	14.9	70.0	16.0	14.0	88.7	11.3	81.8	12.2
Post-treated Cu@PtCu(Gly)	20.5	19.1	15.6	67.7	13.9	18.4	66.3	33.7	66.2	33.8

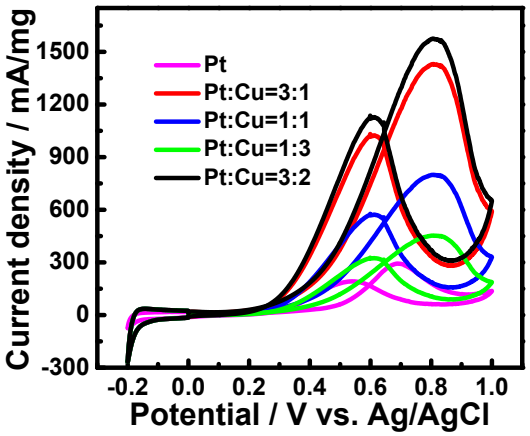

Fig. S1 Cyclic voltammogram of Cu@PtCu(Gly) electrocatalysts prepared under different theoretical molar ratios of Pt:Cu at 1:0, 3:1, 1:1, 1:3, and 3:2 measured in 0.5 M H_2SO_4 + 1 M CH_3OH solution.

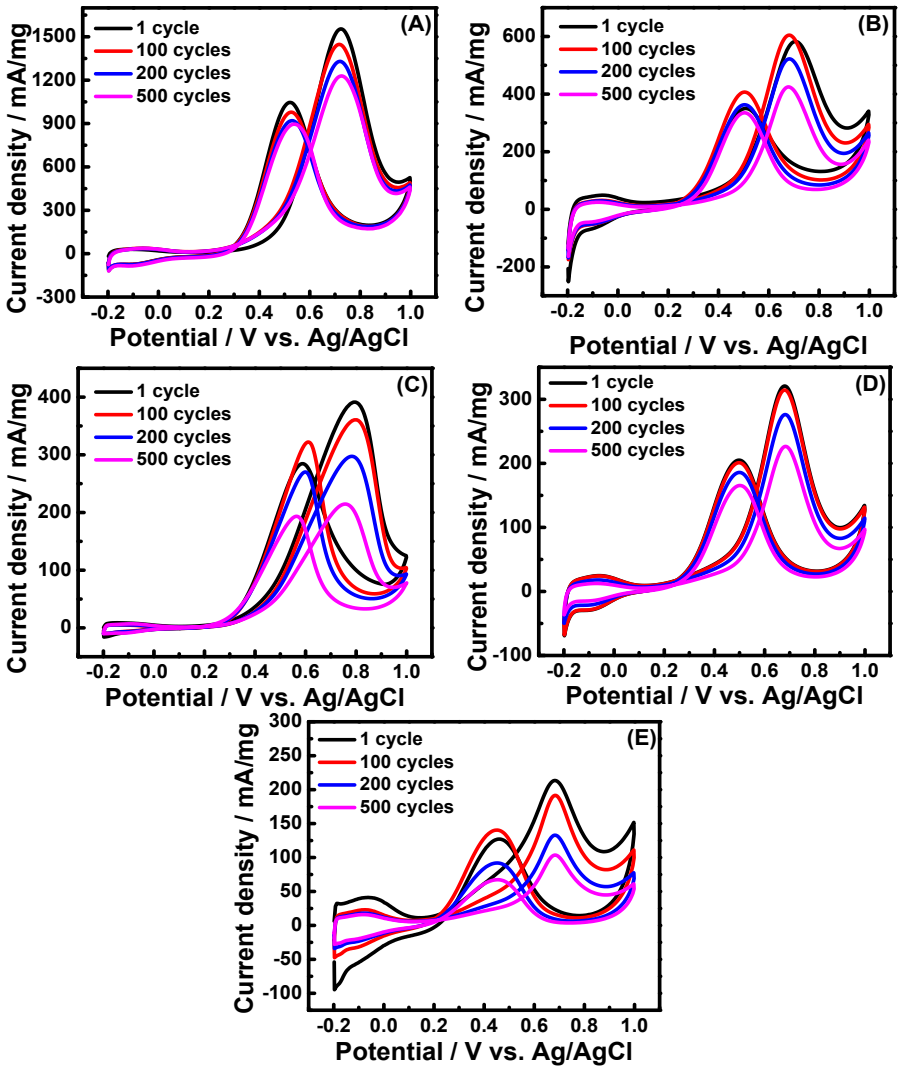

Fig. S2 Cyclic voltammogram of (A) Cu@PtCu(Gly), (B) PtCu(HHA), (C) PtCu(AA), (D) PtCu(SBH) and (E) the commercial Pt/C catalysts measured in 0.5 M H_2SO_4 + 1 M CH_3OH solution with a scan between –0.2 and 1.0 V at a scan rate of 50 mV·s^{-1} after 1, 100, 200 and 500 cycles.

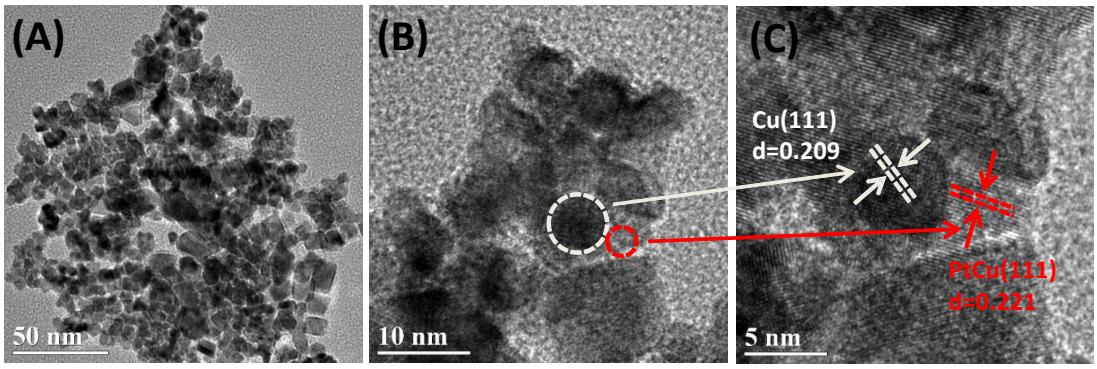

Fig. S3 (a and b) TEM and (c) HRTEM images of Cu@PtCu(Gly) alloy electrocatalyst after the stability test.

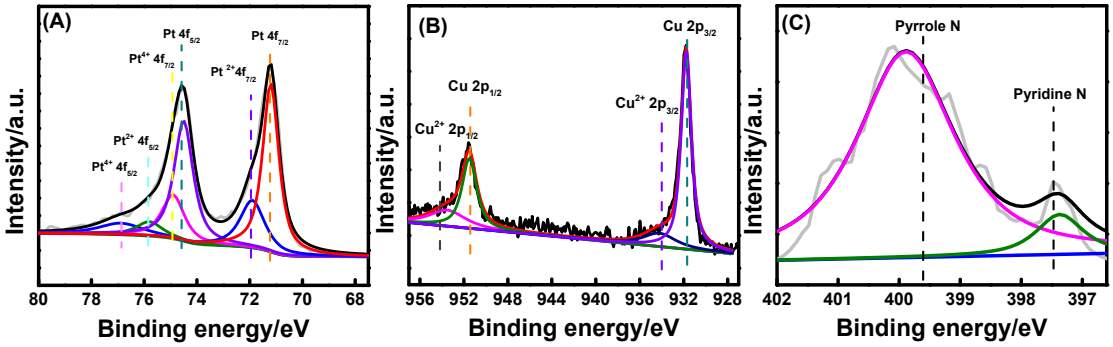

Fig. S4 XPS spectra of (A) Pt 4f, (B) Cu 2p, and (C) N 1s of Cu@PtCu(Gly) alloy electrocatalyst after the stability test.

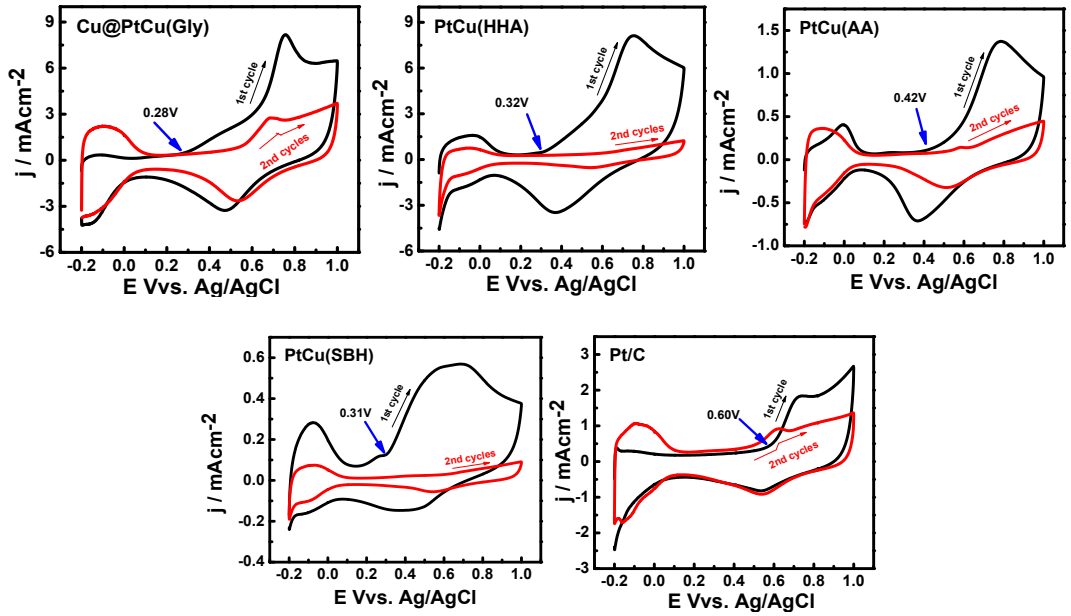

Fig. S5 CO-stripping voltammograms over Cu@PtCu(Gly), PtCu(HHA), PtCu(AA), PtCu(SBH), and the commercial Pt/C electrocatalysts in a CO-saturated 0.5 M H_2SO_4 solution at a scan rate of 50 mV s^{-1}.

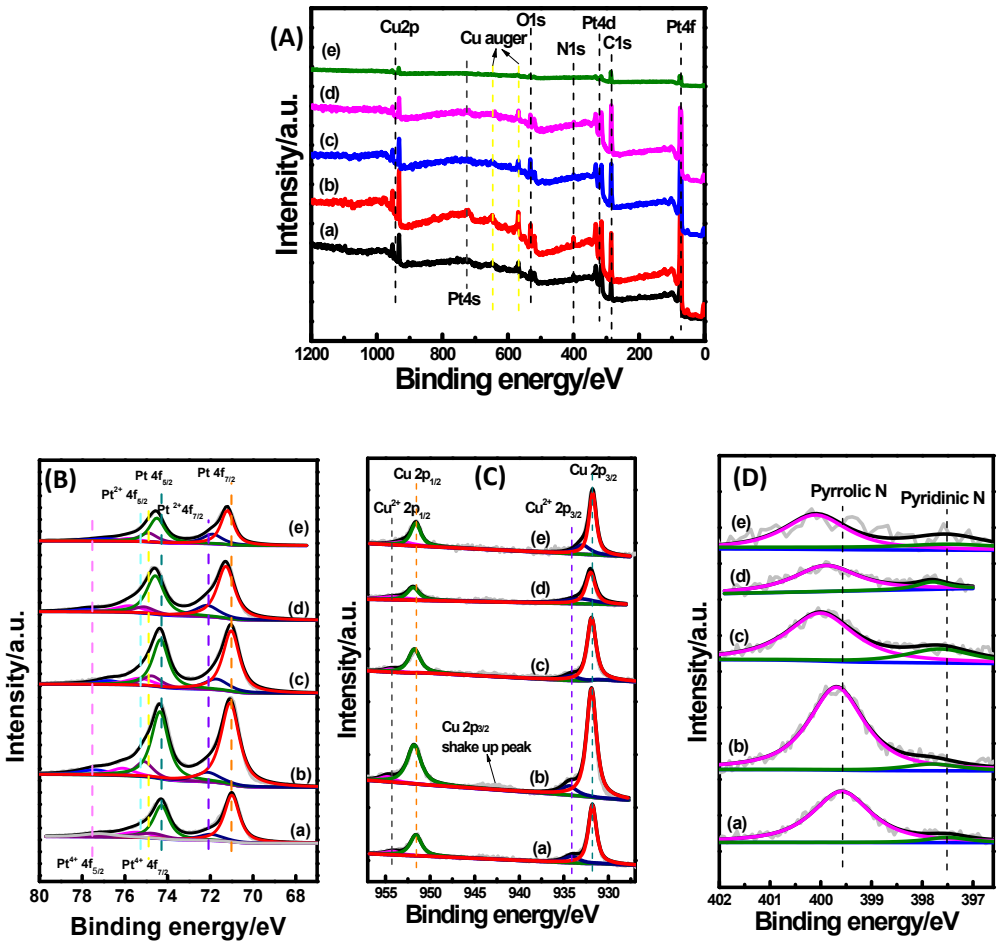

Fig. S6 XPS spectra of (A) survey spectra, (B) Pt 4f, (C) Cu 2p, and (D) N1s of (a) Cu@PtCu Gly, (b) PtCu (HHA), (c) PtCu (AA), (d) PtCu (SBH), and (e) post-treated Cu@PtCu Gly.

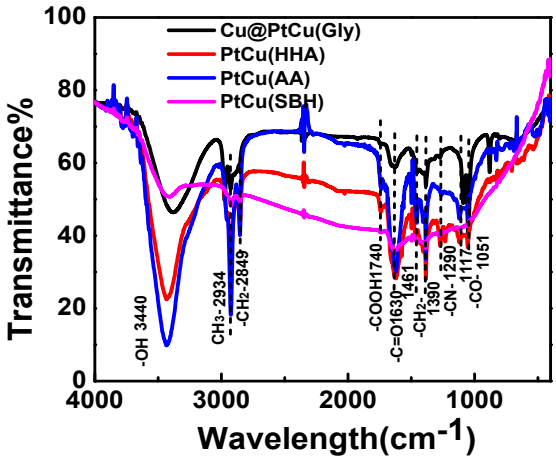

Fig. S7 FI-IR spectra of Cu@PtCu(Gly), PtCu(HHA), PtCu(AA), PtCu(SBH), and the commercial Pt/C electrocatalysts.

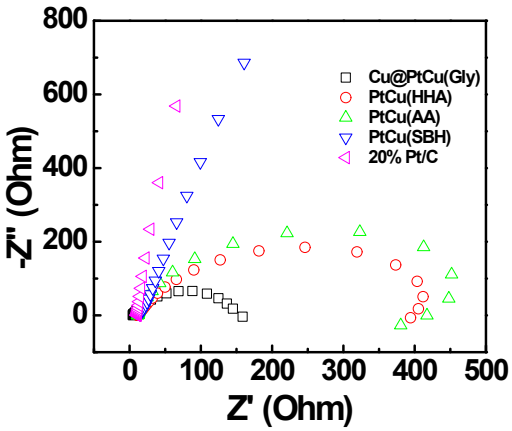

Fig. S8 Electrochemical impedance spectra of Cu@PtCu and PtCu alloy electrocatalysts measured in N_2-saturated 0.5M H_2SO_4 + 1.0M CH_3OH solution.

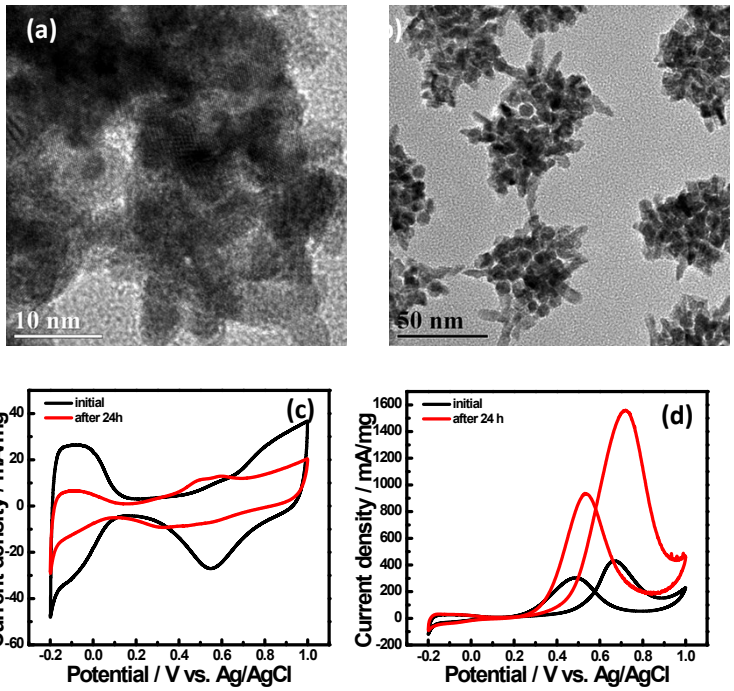

Fig. S9 (a and b) TEM images of Cu@PtCu(Gly) electrocatalyst after being post-treated in a mixture of ethanol and H_2O solvents for 24 h, (c) cyclic voltammogram curves recorded at room temperature in a N_2-saturated 0.5 M H_2SO_4 solution with a scan rate of 100 $mV \cdot s^{-1}$, and (d) comparison of the MOR activity of Cu@PtCu(Gly) electrocatalyst before and after post-treatment.

The post-treatment was utilized to demonstrate that N atoms can be removed from the surface of Cu@PtCu(Gly) electrocatalyst in a mixture of ethanol and H_2O solvents. After post-treatment, the Cu@PtCu Gly nanocrystals still preserve the dendritic core-shell structure as shown in Fig. S9(a and b). The electrocatalytic activities of Cu@PtCu(Gly) electrocatalyst before and after post-treatment was compared. Fig. S2(c) shows the cyclic voltammograms of Cu@PtCu(Gly) electrocatalyst before and after being post-treated in acidic medium (0.5 M H_2SO_4). The double current layer is visibly broader for the Cu@PtCu(Gly) than the post-treated Cu@PtCu(Gly), implying that after post-treatment the Cu@PtCu(Gly) electrocatalyst shows a significant decrease in electrochemically accessible area (ECSA). The ECSA is 44.1 $m^2 \cdot g_{Pt}^{-1}$ and 5.7 $m^2 \cdot g_{Pt}^{-1}$ for the Cu@PtCu(Gly) and the post-treated Cu@PtCu(Gly), respectively. The mass activity of the Cu@PtCu(Gly) electrocatalyst is 1568 $mA \cdot mg^{-1}$ at 0.69 V, which is 3.56 times higher than that of 441 $mA \cdot mg^{-1}$ for the post-treated Cu@PtCu(Gly) electrocatalyst. Such results suggest that the content and species of N element on the surface of the electrocatalyst arisen from the different reduction capability and structural configuration may cause the large variation of the catalytic performance for Cu@PtCu and PtCu alloy electrocatalysts.